Performance of Phasor Measurement Units for Power Quality Event Detection in Urban Distribution Grids

David Macii, Daniele Fontanelli, Dario Petri
Department of Industrial Engineering
University of Trento, Trento, Italy
E-mail: david.macii@unitn.it, daniele.fontanelli@unitn.it, dario.petri@unitn.it

***Abstract* — In densely populated urban areas, the increasing variability of power supply and demand due to the presence of a multitude of prosumers will greatly affect power quality (PQ). In order to monitor the state of distribution systems, a larger number of Phasor Measurement Units (PMU) is expected to be deployed in the next future. However, to what extent PMU algorithms (especially those used in P Class instruments) can actually detect typical PQ events and can replace or integrate existing PQ meters is still unclear. The goal of this paper is to investigate this issue and to provide a preliminary overview of the role of PMUs for voltage dips and swells detection. The proposed analysis relies on a simulation-based performance comparison between two PMU algorithms (provided with an additional median filter) and the classic technique relying on zero-crossing detection and true Root Mean Square (RMS) magnitude estimation. All simulations have been performed in realistic conditions, assuming to acquire voltage waveforms compliant with the EN Standard 50160:2010 and affected by dips or swells of different amplitude and duration. Even if no experimental data are collected on the field, the proposed analysis provides a useful insight into the potentialities and limitations of PMU algorithms for voltage dips and swells detection.**

***Keywords* — Power Quality monitoring (PQ), phasor measurement units (PMUs), smart grids, smart cities.**

I. Introduction

As known, enhanced energy efficiency [1], [2], smart grid evolution [3], [4] and electrical mobility [5], [6] are key elements for the development of sustainable smart cities [7]. Unfortunately, such elements are also expected to exacerbate power quality (PQ) issues. As defined in the IEEE Standard 1159-2009 "the term *power quality* refers to a wide variety of electromagnetic phenomena that characterize voltage and current at a given time and at a given location on the power system [8]." In general, two kinds of PQ phenomena exist, i.e.

- Continuous or prolonged variations of voltage or current waveform characteristics;
- Occasional and sudden deviations (usually referred to as *events*) of voltage or current waveforms from their nominal shape.

PQ-related problems have steadily grown over the last twenty years. This is due to the widespread use of non-linear equipment and appliances that distort the current profiles and affect grid voltage as well [9]. Recently, the European Energy Efficiency Directive (EED) 2012/27/EU has further accelerated this trend. For instance, the progressive replacement of:

- Incandescence lamps with LED-based or compact fluorescent lamps;
- Standard drives and pumps with variable speed drives;
- Classical oil or gas heating facilities with electrical heat pumps and
- Ordinary street lighting systems with smart light posts controllable through Power Line Communications (PLC);

not only helps to reduce greenhouse gas emissions and energy consumption in cities, but it also causes an increment in the level of oscillations, harmonics and flicker over urban distribution networks. In addition, the potential simultaneous connection and disconnection of a large number of distributed generators and electric vehicles could seriously undermine power grid stability due to large power imbalances, that could strongly affect PQ [9], [10].

In order to ensure adequate PQ levels with adequate reliability, and to prevent possible harmful consequences on electronic systems, a multitude of PQ monitoring techniques have been proposed in the last years, e.g. to measure flicker, harmonics and inter-harmonics, and to detect events such as voltage interruptions, dips/sags and swells [11]-[16]. Such phenomena have a strong economic impact on production lines, as well.

At the moment, the main reference technical documents adopted in Europe for PQ monitoring are the IEC Standards 61000-4-7:2012 for harmonic and inter-harmonic measurement [17], 61000-4-15:2010 for flicker measurement [18], and 61000-4-30:2015 specifically for dips and swells detection [19]. However, it is not clear whether existing systems and techniques are accurate or fast enough to meet the requirements of future distribution networks. In this context, some researchers have recently proposed to combine the features of traditional PQ meters with those of other instruments, such as the so-called Phasor Measurement Units (PMUs). These instruments are able to measure magnitude, phase, frequency and rate of change of frequency (ROCOF) of voltage or current waveforms synchronized to the Universal Coordinated Time (UTC) [20], [21]. Originally designed as high-end instruments for transmission systems [22], nowadays simpler and cheaper PMUs incorporating PQ monitoring capabilities have become appealing also at the distribution level [23], e.g. to detect voltage and frequency disturbances at

978-1-5090-1846-8/16/$31.00 ©2016 IEEE

sensitive loads [24]. While standard PMUs can hardly measure the parameters of strongly distorted waveforms with adequate accuracy [20], the potentialities of PMUs for PQ event detection (especially the P Class instruments which are conceived for protection purposes) are still quite unexplored. So, the aim of this paper is to investigate the ability of PMUs to detect voltage dips or swells using two well-established techniques, i.e. the so-called Interpolated Discrete Fourier Transform (IpDFT) [25], which relies on a static phasor model, and the Taylor Weighted Least Squares (TWLS) algorithm (sometimes called also as Taylor Fourier Filter - TFF), which instead is based on a dynamic (i.e. time-varying) phasor model [26], [27].

The rest of the paper is structured as follows. In section II, the main features of voltage dips and swells are shortly described. Section III recalls the IpDFT and the TWLS algorithm as well as the classic RMS-based approach mentioned in the IEC Standard 61000-4-30:2015. Finally, in Section IV the performances of these techniques are compared through simulations.

II. Voltage Dips and Swells Description

In [19] a *voltage dip* (also referred to as a *voltage sag* in the IEEE Standard 1159:2009 [8]) is defined as "a temporary reduction of the voltage at a point in the electrical system below a threshold." Such a reduction can be caused by a short circuit or an earth fault close to substations. However, voltage reductions may arise also when large motors start or because of sudden load increments. Usually, voltage dips last for a short amount of time (ranging from half a cycle to some seconds), till when some proper counteraction is taken (e.g., load stabilization and balancing or fault mitigation). Of course, longer dips (in the order of up to 1 minute) are also possible. According to standard PQ taxonomy, the voltage root mean square (RMS) magnitude of a dip never drops to zero. These kinds of events are instead referred to as *interruptions*. In any case, to detect both dips and interruptions, a suitable threshold T_1 (defined as a fraction of the nominal input RMS voltage or of the average RMS voltage over a certain time interval) has to be chosen. For statistical applications or troubleshooting, the value of T_1 usually ranges between 85%-90% of the reference voltage. For contractual applications instead T_1 is set equal to 70% of the reference voltage.

In general, dips have to be detected quickly and with a high level of confidence. In the following, we will refer to *dip detection latency* as the time difference between the instant when the voltage RMS magnitude measured by a PQ meter is lower than or equal to T_1 and the time when the dip actually occurs. The main parameters of interest of a voltage dip are:

- The *residual voltage*, namely the lowest RMS magnitude during the event;
- The *depth of the dip*, i.e. the difference between the reference voltage and the residual voltage, expressed as a percentage of the reference voltage;
- The *dip duration*, i.e. the time difference between the instant when the voltage RMS magnitude is lower than or equal to T_1 and the moment when it becomes greater than another threshold T_2. Such a threshold is purposely set larger than T_1 to avoid multiple spurious detections. In particular, the hysteresis magnitude is usually 2% of the reference voltage [19].

It is worthwhile to remind that in polyphase systems a dip refers to any voltage reduction below T_1 occurring over any one of the available lines. In such cases, a dip ends when the voltage RMS magnitude over all the phases rise above T_2. It is also important to notice that real dips may include not only voltage envelope variations, but also significant phase shifts.

The dual phenomenon of a voltage dip is the so-called *voltage swell*, i.e. "a temporary increase of the voltage at a point in the electrical system above a threshold" [19]. In general, voltage swells are much less common than dips and may occur on unfaulty phases because of earth faults, when large loads are switched off or when large capacitor banks are turned on. The *duration* of a swell is defined as the length of the time interval between the moment when the voltage magnitude exceeds a threshold T_3 (generally set to 110% of the reference voltage) and the instant when the voltage RMS magnitude decreases below threshold T_4. This is typically given by T_3 minus a hysteresis of magnitude equal to a 2% of the reference voltage [19]. Again, the *swell detection latency* is the time difference between the instant when the voltage RMS magnitude measured by a PQ meter becomes greater than or equal to T_3 and the time when the swell actually occurs. During this event, the main parameter of interest is the *maximum voltage RMS magnitude*.

III. Algorithms for Voltage Dips and Swell Detection

Let f_s and r be the instrument sampling rate and the time index of a data record during which a dip or a swell occurs. If this observation interval consists of N samples, the digitized voltage waveform for $n = r\text{-}N\text{+}1,\ldots,r$ can be modeled as

$$x_r(n) = \sqrt{2}\left[A + s_a(n)\right]\cos\left[2\pi\frac{f_0(1+\varsigma)}{f_s}n + \varphi\right] + \varepsilon_h(n) + \varepsilon_w(n) \quad (1)$$

where A is the wanted voltage RMS magnitude, f_0 is the nominal waveform frequency, ς is the static off-nominal fractional frequency offset, φ is the initial phase of the fundamental, $\varepsilon_h(\cdot)$ is a discrete-time sequence including both harmonic and inter-harmonic terms, $\varepsilon_w(\cdot)$ is the additive wideband noise (e.g. introduced by analog front-end circuitry and the analog-to-digital converter) and finally,

$$s_a(n) = \begin{cases} A_{ds} & \text{if an event occurs at sample } n \\ 0 & \text{otherwise} \end{cases} \quad (2)$$

denotes the potential voltage variation occurring at sample n due to the dip ($A_{ds}<0$) or to the swell ($A_{ds}>0$).

In the following, three algorithms for dip/swell measurements are shortly recalled and described, i.e. the classic approach mentioned also in the IEC Standard 61000-4-30 [19], the IpDFT algorithm [25], and the TWLS technique [26], [27].

A. Classic RMS algorithm

The classic approach for PQ dip/swell detection consists essentially of three steps. First, the zero crossings of the fundamental have to be found. In order to avoid multiple zero crossings, harmonics, inter-harmonics and noise have to be suitably attenuated. In the implementation used in this paper, a plain band-pass filter with a unit gain and a 10-Hz -3dB bandwidth centered in f_0 has been used.

Once the zero crossings are detected, voltage dip or swell measurements rely on the computation of the true RMS value over an integer number C of cycles, i.e.

$$\hat{X}_{RMS}(r)=\sqrt{\frac{1}{|W(0)|}\sum_{n=z_{r0}}^{z_{rC}}[w(n)x_r(n)]^2} \qquad (3)$$

where z_{r0} and z_{rC} are the indexes corresponding to the first and to the last zero-crossing samples within data record (1), $w(\cdot)$ represents the adopted window function and $|W(0)|$ is the window DC gain. It is important to emphasize that in the IEC Standard 61000-4-30 [19], C must be equal to 1 and $w(\cdot)$ is implicitly assumed to be a rectangular window. Therefore, $|W(0)|=N$. However, in this paper also the results over C=2 cycles using a Hann window are reported, as such settings are closer to the operating conditions of P-Class PMUs.

In the last step of the algorithm, i.e. after the RMS magnitude is estimated through (3), dip or swell detection simply relies on the comparison between $\hat{X}_{RMS}(r)$ and T_1 or T_3, respectively. Similarly, the end of an event is detected whenever $\hat{X}_{RMS}(r)$ exceeds T_2 or T_4.

B. IpDFT algorithm

The IpDFT algorithm relies on the Windowed Discrete Fourier Transform (WDFT). However, unlike the basic WDFT estimator, the magnitude error due to the scalloping loss of the chosen window in the frequency domain is properly estimated and compensated. If f_s is not an integer multiple of f_0 (i.e. $\varsigma\neq 0$), the actual number of observed cycles is not exactly an integer number C. As a result, the spectral peak of the fundamental component does not lie exactly at the C-th frequency bin and the RMS magnitude estimated in the center of record (1) is given by [25]

$$\hat{X}_{IpDFT}(r)=\frac{\sqrt{2}N|X_{w_r}(C)|}{|W(-\hat{\delta}_r)|}, \qquad (4)$$

where $|X_{w_r}(C)|$ is the C-th spectral sample of the WDFT, $|W(\cdot)|$ is the magnitude of the discrete-time Fourier frequency transform of the chosen window function, and, finally, δ_r results from the solution of [25]

$$\frac{|X_{w_r}(C+i)|}{|X_{w_r}(C-1+i)|}\cong\frac{|W(i-\delta_r)|}{|W(-1+i-\delta_r)|}. \qquad (5)$$

Note that in (5), when C = 1, then i must be equal to 1 to avoid the use of the DC component, which is strongly affected by the infiltration of the image component of the fundamental. On the contrary, when C > 1, then i = 0 if $|X_{w_r}(C-1)|\geq|X_{w_r}(C+1)|$ or i = 1 if $|X_{w_r}(C-1)|<|X_{w_r}(C+1)|$.

In principle, for voltage dip or swell detection the result of (4) should be compared with T_1 and T_2 or T_3 and T_4, respectively. However, the phasors estimated during step-like changes can be affected by large overshoots and undershoots [28], which in turn may degrade detection probability. In order to solve this problem a one-cycle median filter can be applied before threshold comparison. This approach greatly improves detection probability, although it also increases detection latency, as it will be shown in Section IV.

C. TWLS algorithm

The TWLS algorithm relies on the Taylor's series expansion of the waveform phasor (regarded as a function of time) till a given order K. One of the main advantages of this approach is that if $K\geq 2$, waveform magnitude, angle, frequency and ROCOF in the center of an observation interval can be estimated in one shot using a weighted least squares approach [26], [27]. In particular, with reference to (1), if $\overline{\boldsymbol{X}}_{r_K}=\left[X^*_{r_K}X^*_{r_{K-1}}\ldots X^*_{r_0}\,X_{r_0}\ldots X_{r_{K-1}}\,X_{r_K}\right]^T$ is the vector containing the complex conjugate pairs of phasor Taylor's series coefficients (namely the parameters to be estimated) it follows that

$$\hat{\overline{\boldsymbol{X}}}_{r_K}=2\left(A_K^H\Omega^H\Omega A_K\right)^{-1}A_K^H\Omega^H\Omega\,\boldsymbol{x}_r, \qquad (6)$$

where $\boldsymbol{x}_r$ is the column vector of the data record (1), Ω is a diagonal matrix including the coefficients of the chosen window $w(\cdot)$, $\cdot^*$ and $\cdot^H$ denote the conjugate and Hermitian operators, respectively, and A_K is the $N\times 2(K+1)$ system matrix (reported for instance in [28]) describing the linear relationship, in the time domain, between the waveform samples and the Taylor's series coefficients. Note that the voltage RMS magnitude of the fundamental results simply from

$$\hat{X}_{TWLS}(r)=|X_{r_0}|. \qquad (7)$$

Again, the estimation errors during transients in the case of step-like amplitude or phase changes can be quite large [30], and may cause multiple spurious crossings of the detection thresholds, thus undermining event detection probability. However, also in this case, this problem can be effectively solved by applying a one-cycle median filter to (7) and by comparing the filter output with T_1 and T_2 or with T_3 and T_4 for dip and swell detection, respectively.

IV. Simulation Results

In order to analyze and to compare the performances of the algorithms described in Section III, several Monte Carlo simulations in different conditions have been performed in Matlab. In all cases, the collected voltage waveforms are assumed to meet the basic requirements of low-voltage (LV) distribution systems reported in the Standard EN 50160:2010 [29]. In particular, with reference to the waveform model (1), the following simulation parameters have been used.

- The nominal frequency f_0=50 Hz is affected by static fractional off-nominal frequency offsets ς normally distributed within ±1% of f_0 with 99.7% probability;
- The nominal voltage RMS waveform magnitude is set equal to A = 1 p.u. Dips and swells are assumed to occur always at the same time with relative RMS magnitude A_{ds} ranging between -90% and -10% of A for dips or between 10% and 80% for swells.
- Event duration ranges from 0.5 to 30 waveform cycles. The chosen values of amplitude and duration are compliant with the definition of "instantaneous" dips and swells reported in the IEEE Standard 1159:2009 [8]. Longer events (i.e. referred to as "momentary" or "temporary" in IEEE Standard 1159:2009) are not considered explicitly in the following, as they are certainly easier to detect than the "instantaneous" ones.
- In order to evaluate the effect of different angle values on dip or swell detection, φ is swept linearly in [0,2π[. In particular, 50 phases are considered for each value of dip/swell magnitude and duration.
- f_s is set equal to 6.4 kHz. In this way, 128 samples per nominal cycle are collected, as recommended in clause A.9.1 of [19] for fast event detection;
- $\varepsilon_h(n)$ is given by the superimposition of 25 harmonics with phases chosen randomly with uniform distribution in [0,2π[and magnitudes equal to the maxima reported in Table 1 of the Standard EN 50160 [29].
- Finally, the variance of $\varepsilon_w(n)$ is computed under the assumption that the Effective Number of Bits (ENOB) of the acquisition front-end is about 12 bits, which is a realistic feature for existing instruments.

Fig. 1 shows the probabilities of detecting half-cycle-long voltage dips (a) or swells (b) as a function of A_{ds} over one-cycle (C=1) rectangular windows or two-cycle (C=2) Hann windows using the algorithms considered. The threshold values in either case are T_1 = 0.9 p.u. and T_2 = 0.92 p.u. for dip detection or T_3 = 1.1 p.u. and T_4 = 1.08 p.u. for swell detection, respectively, in compliance with the requirements of [19]. Observe that if C=1 and the dip/swell magnitude exceeds ±30% of the reference voltage level, the probability of detection is about 100%. However, when smaller dips and swells occur, the classic RMS-based approach performs better than the solutions based on PMU algorithms with median filters. On the other hand, when C=2, the probabilities of detecting dips and swells are globally worse, but the TWLS-based approach is more reliable than the other techniques taken into consideration.

It is worth emphasizing that the results shown in Fig. 1 refer to worst-case testing conditions, i.e. under the effect of significant disturbances and when dips and swells are very short, i.e. shorter than algorithms transient duration. On the contrary, when dip or swell duration is longer than one cycle, all algorithms have enough time to reach a steady state before the event ends. In such situations, the detection probability always approaches 100%, regardless of both the estimation algorithm and the observation interval length.

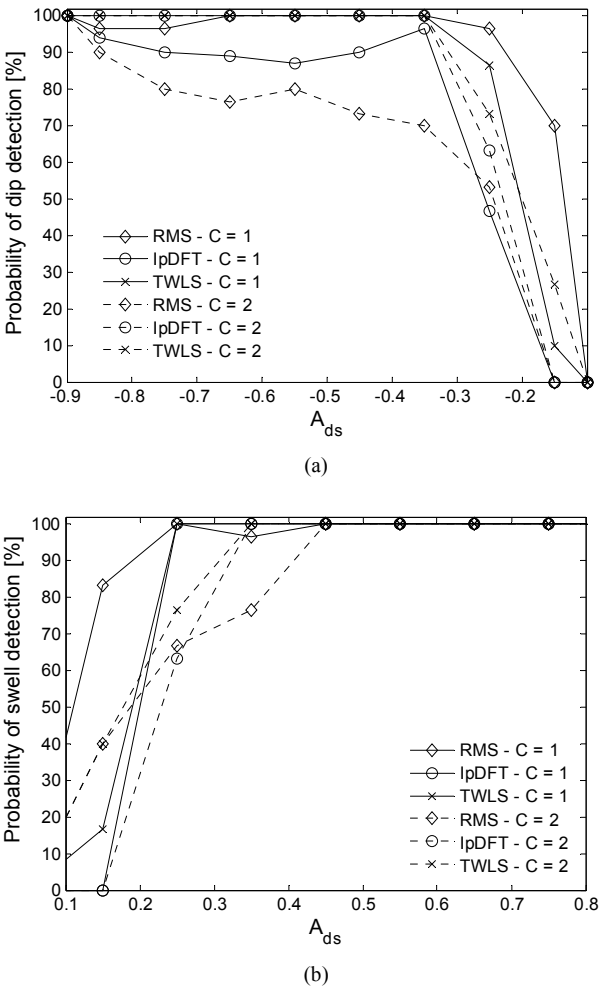

Fig. 1 – Probabilities of detecting half-cycle-long voltage dips (a) or swells (b) as a function of A_{ds}. Different markers refer to the three estimation algorithm considered in this paper (i.e. classic RMS, IpDFT and TWLS with a half-cycle refresh rate). Solid and dotted lines refer instead to one-cycle and two-cycle observation intervals using rectangular and Hann windows, respectively.

Fig. 2(a)-(b) shows an example of a voltage dip with a residual RMS magnitude equal to 25% of the reference value and a duration of 0.5 s. In (a) the nominal RMS magnitude of the whole voltage dip is shown (thick dotted line) along with the envelopes estimated by changing φ. All results have been obtained using the three algorithms described in Section III over one-cycle rectangular windows sliding sample-by-sample. Fig. 2(b) displays a zoomed portion of the envelopes around the falling edge of the dip aligned on a common time-scale, i.e. after compensating the systematic detection latencies (which are instead reported in Tab. I). In both pictures the two horizontal dotted lines represent thresholds T_1 and T_2. As explained in Section III, the results obtained with the TWLS and the IpDFT estimators are shown after applying the median filter, which greatly improves detection robustness. The time intervals delimited by the intersection points between the magnitude envelopes and threshold T_1 give an idea of the worst-case detection jitter of each algorithm. At a glance, the jitter of TWLS-based and IpDFT-based dip

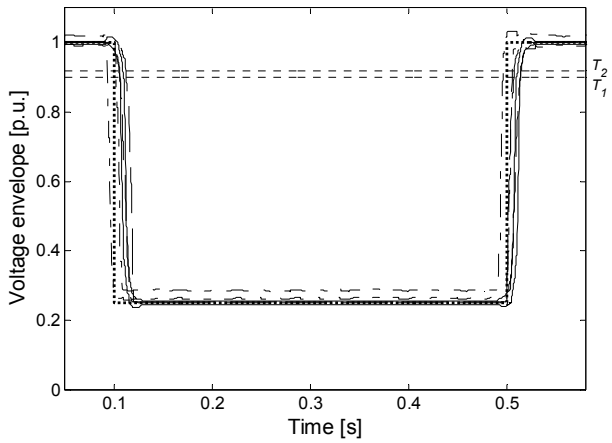

(a)

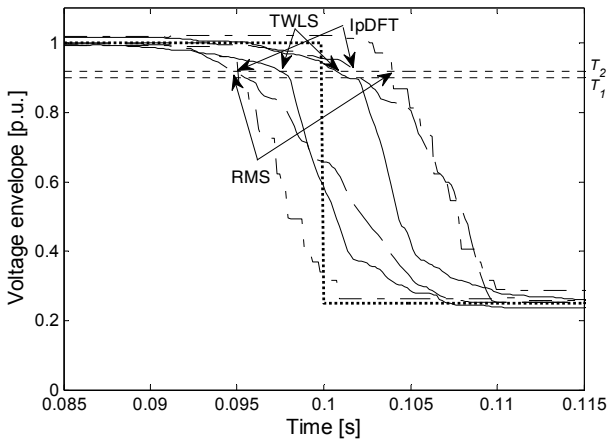

(b)

Fig. 2 – Example of a voltage dip with a residual RMS magnitude equal to 25% of the reference value and a duration of 0.5 s. In (a) the voltage dip is shown along with the envelopes estimated by the TWLS and IpDFT algorithms (with an output median filter) and by the standard RMS-based technique over a one cycle rectangular window sliding sample-by-sample. In (b) a zoomed portion of the envelopes around the dip falling edge is displayed. All curves are aligned on the same timescale.

detection is smaller than the jitter introduced by the classic RMS-based technique. Indeed, the last approach is inherently affected by the half-cycle synchronization uncertainty due to the zero-crossing detection mechanism described in [13].

Tab. I reports the mean values and the standard deviations of the detection latencies (expressed in nominal waveform cycles) for dips with a different depth. The dual results in the case of voltage swells are very similar and are not reported for the sake of brevity. The values in Tab. I are first estimated over one-cycle or two-cycle observation intervals sliding sample-by-sample, using a rectangular or a Hann window, respectively, and changing the initial phases at the beginning of each run. Then, the mean values and the standard deviations computed over 50 trials and obtained with dips lasting from 0.5 to 30 cycles are averaged together to improve estimation accuracy (latency fluctuations are indeed quite independent of dip duration).

Observe that the mean (i.e. systematic) detection latencies of the PMU algorithms are significantly longer than those obtained with the RMS-based approach, mainly because of the output median filter. Notice also that in all cases the mean detection latencies become shorter as the depth of the dip grows. On the contrary, the latency standard deviations are quite independent of dip magnitude and those of PMU algorithms are much smaller (from ⅓ to ½) than those obtained with the classic RMS-based technique. Thus, we can finally conclude that, even if PMUs globally require a longer detection time, they are more accurate in reconstructing (a posteriori) when an event actually occurred, i.e. after the systematic contributions are estimated and compensated.

Tab. II shows the mean values and the standard deviations of the dip duration estimation errors. All values in Tab. II are computed like those in Tab. I. Again, they are expressed in nominal waveform cycles for dips with a different depth. The results about swells are very similar; so again they are not reported for the sake of brevity. Notice that all algorithms introduce a bias that tends to grow almost monotonically as the dip residual voltage decreases. Moreover, for a given depth, the bias is larger when C=2. Apparently, the minimum biases are achieved using the RMS-based detection algorithm over one cycle. However, the corresponding standard deviation values are from about two to four times larger than those obtained with the PMU algorithms. Since all biases can be compensated once the residual voltage is measured, the event duration estimated using the PMU algorithms can be more accurate than the duration accuracy achieved with the RMS-based technique, although the former may require some additional processing. Of course, the above considerations hold only in the case of sample-by-sample estimates. If the RMS magnitude estimates are updated every half-cycle (which is the default setting specified in [19]) both detection latency and event duration uncertainties are multiples of the update period. So the differences between algorithms can be hardly appreciated in this case.

Tab. III shows the mean values and the standard deviations of the residual voltage relative estimation errors (updated every half-cycle) for dips characterized by different depth and duration. In this case, for the sake of brevity, just the results over one cycle with a rectangular window are reported. This choice is motivated by the fact that using two-cycle observation intervals does not bring any significant benefit in terms of either event detection probability or timing accuracy. Observe that, in the case of dips shorter than one cycle, results are very inaccurate, as they are strongly affected by algorithm transients. For dips longer than one cycle instead, the residual voltage estimation accuracy of all algorithms tends to become independent of event duration. This is reasonable, since in such cases the voltage magnitude is estimated in steady-state conditions. Quite interestingly, the TWLS algorithm tends to underestimate the actual magnitude, while the IpDFT returns the most accurate results. The classic RMS technique instead exhibits the strongest dependence on the actual residual voltage. Note that most of the values reported in Tab. III are well beyond the Class A measurement uncertainty interval specified in [19] (i.e. ±0.2%). However, this is not in contradiction with the requirements of the Standard, as the

TABLE I – MEAN VALUES μ AND STANDARD DEVIATIONS σ OF THE VOLTAGE DIP DETECTION LATENCIES (EXPRESSED IN NUMBER OF NOMINAL WAVEFORM CYCLES AT 50 HZ) FOR EVENTS OF DIFFERENT DEPTH. THE REPORTED VALUES ARE ESTIMATED USING THREE DIFFERENT ALGORITHMS OVER ONE CYCLE (WITH A RECTANGULAR WINDOW) AND TWO CYCLES (WITH A HANN WINDOW). THE VOLTAGE MAGNITUDE ESTIMATES ARE UPDATED 128 TIMES PER CYCLE, AS SUGGESTED IN CLAUSE A.9.1 OF THE STANDARD IEC 61000-4-30.

A_{ds}/A [%]	TWLS with median filter				IpDFT with median filter				RMS			
	C=1 (rectangular)		*C*=2 (Hann)		*C*=1 (rectangular)		*C*=2 (Hann)		*C*=1 (rectangular)		*C*=2 (Hann)	
	μ [cycles]	σ [cycles]	μ [cycles]	σ [cycles]	μ [cycles]	σ [cycles]	μ [cycles]	σ [cycles]	μ [cycles]	σ [cycles]	μ [cycles]	σ [cycles]
-15	1.10	0.08	1.10	0.07	-	-	-	-	0.61	0.15	1.28	0.15
-35	0.98	0.07	1.49	0.06	0.92	0.08	1.33	0.06	0.50	0.15	1.08	0.15
-55	0.94	0.06	1.43	0.06	0.90	0.09	1.22	0.06	0.47	0.15	1.04	0.15
-75	0.92	0.06	1.39	0.06	0.94	0.10	1.15	0.06	0.46	0.15	1.00	0.15
-95	0.90	0.04	1.34	0.06	0.94	0.09	1.10	0.06	0.44	0.15	0.95	0.15

TABLE II – MEAN VALUES μ AND STANDARD DEVIATIONS σ OF THE VOLTAGE DIP DURATION ESTIMATION ERRORS (EXPRESSED IN NUMBER OF NOMINAL WAVEFORM CYCLES AT 50 HZ) FOR EVENTS OF DIFFERENT DEPTH. THE REPORTED VALUES ARE ESTIMATED USING THREE DIFFERENT ALGORITHMS OVER ONE CYCLE (WITH A RECTANGULAR WINDOW) AND TWO CYCLES (WITH A HANN WINDOW). THE VOLTAGE MAGNITUDE ESTIMATES ARE UPDATED 128 TIMES PER CYCLE, AS SUGGESTED IN CLAUSE A.9.1 OF THE STANDARD IEC 61000-4-30.

A_{ds}/A [%]	TWLS with median filter				IpDFT with median filter				RMS			
	C=1 (rectangular)		*C*=2 (Hann)		*C*=1 (rectangular)		*C*=2 (Hann)		*C*=1 (rectangular)		*C*=2 (Hanning)	
	μ [cycles]	σ [cycles]	μ [cycles]	σ [cycles]	μ [cycles]	σ [cycles]	μ [cycles]	σ [cycles]	μ [cycles]	σ [cycles]	μ [cycles]	σ [cycles]
-15	-0.10	0.10	-0.09	0.06	-0.32	0.12	-0.21	0.04	-0.10	0.18	-0.19	0.19
-35	0.16	0.08	0.23	0.06	0.31	0.11	0.48	0.04	0.11	0.20	0.17	0.22
-55	0.24	0.08	0.33	0.06	0.29	0.12	0.70	0.04	0.15	0.23	0.40	0.20
-75	0.29	0.07	0.38	0.06	0.20	0.12	0.82	0.04	0.17	0.25	0.49	0.13
-95	0.33	0.06	0.42	0.06	0.45	0.10	0.91	0.04	0.19	0.25	0.51	0.15

TABLE III – MEAN VALUES μ AND STANDARD DEVIATIONS σ OF THE RELATIVE ESTIMATION ERRORS OF DIP RESIDUAL VOLTAGES FOR EVENTS OF DIFFERENT DEPTH AND DURATION. ALL MAGNITUDES ARE ESTIMATED OVER ONE-CYCLE INTERVALS (WITH A RECTANGULAR WINDOW) AND ARE UPDATED EVERY HALF CYCLE.

Duration [cycles]	A_{ds}/A [%]	TWLS		IpDFT		RMS	
		C=1 (rect.)		*C*=1 (rect.)		*C*=1 (rect.)	
		μ [%]	σ [%]	μ [%]	σ [%]	μ [%]	σ [%]
0.5	**-25**	8	4	11	4	15	2
	-55	18	7	25	9	39	6
	-85	30	13	40	14	45	15
1	**-25**	1	3	0.3	0.2	3.7	0.8
	-55	-1	3	0.5	0.3	0.3	0.3
	-85	-2	3	0.9	0.5	0.7	0.4
5	**-25**	-2	2	0.1	0.1	3.1	0.4
	-55	-3	3	0.1	0.1	0.4	0.3
	-85	-2	2	0.1	0.1	0.6	0.3

results in Tab. III are obtained under the effect of realistic disturbances, as explained at the beginning of this Section. If the same simulations were repeated in ideal conditions (i.e. with a pure sinewave at the nominal frequency not affected by noise and harmonics), the mean values and the standard deviations of the residual voltage estimation errors would be negligible for all algorithms, except in the case of events shorter than one cycle.

V. CONCLUSIONS

The increasing penetration of distributed generators and large time-varying loads (e.g. electric vehicles) are expected to greatly affect power quality (PQ) over distribution networks, especially in large urban areas where the concentration of prosumers is steadily growing. The Phasor Measurement Units (PMUs) are instruments able to measure synchronously (i.e. on a common timescale) waveform magnitude, phase, frequency and ROCOF in different points of a network, thus greatly improving grid state estimation, network observability and fault detection capability. Even if some researchers envision a massive deployment of low-cost PMUs at the distribution level, it is known that these instruments have not been conceived for PQ monitoring. So, it can be interesting to evaluate to what extent PMUs (especially the so-called P Class instruments) can side, complement or even replace existing PQ meters for voltage dip and swell detection. Even if no experimental data are available at the moment, assuming that the measurement uncertainty contributions different from those due to signal processing are the same in all cases, the simulation-based analysis reported in this paper shows that some classic static and dynamic synchrophasor estimation algorithms (properly combined with a median filter) can reliably detect dips and swells in realistic conditions. In particular, the uncertainty associated with the estimation of dips or swells magnitude using the PMU algorithms is comparable with that achievable using the standard technique based on zero-crossing detection and true RMS magnitude computation. However, the latter approach seems to be more effective when events characterized by small under- or over-voltages and duration shorter than one cycle occur. In terms of response time and time interval measurement accuracy, the PMUs algorithms can exhibit longer detection latencies and may introduce slightly larger systematic biases. However, such biases can be compensated and the jitter affecting both event detection and dip/swell duration measurement is much

smaller than using the classic RMS-based approach. In conclusion, even if it seems not to be worthwhile to deploy PMUs just for PQ event detection, these instruments could be adapted to perform this additional task along with their traditional functions. Of course, further research activities based on experiments on the field are needed to confirm the validity of this preliminary analysis.

REFERENCES

[1] M. Bertoncini, "Multi-resource optimized smart management of urban energy infrastructures for improving smart city energy efficiency," Proc. *Int. Conference on Smart Cities and Green ICT Systems (SMARTGREENS),* Lisbon, Portugal, May 2015, pp. 1-8.

[2] J. R. Galvão, L. M. Moreira, R. M. T. Ascenso and S. A. Leitão, "Energy systems models for efficiency towards Smart Cities," Proc. *IEEE International Conference on Computer as a Tool (EUROCON),* Salamanca, Spain, Sep. 2015, pp. 1-6.

[3] M. Curiale, "From smart grids to smart city," *2014 Saudi Arabia Smart Grid Conference (SASG),* Jeddah, Saudi Arabia, Dec. 2014, pp. 1-9.

[4] A. C. Becerra, W. Zeng, M. Y. Chow and J. J. Rodríguez-Andina, "Green city: A low-cost testbed for distributed control algorithms in Smart Grid," Proc. *Annual Conference of the IEEE Industrial Electronics Society* (IECON), Yokohama, Japan, Nov. 2015, pp. 1948-1953.

[5] E. Couzineau-Zegwaard, M. Barabel and O. Meier, "From smart grid to smart city business ecosystem: Strategy to define the proper legitimacy for an energy utility firm," Proc. *2013 World Electric Vehicle Symposium and Exhibition (EVS27)*, Barcelona, Spain, Nov. 2013, pp. 1-11.

[6] W. Shuai, P. Maillé, A. Pelov, "Charging Electric Vehicles in the Smart City: A Survey of Economy-Driven Approaches," *IEEE Transactions on Intelligent Transportation Systems*, vol. PP, no. 99, 2016, pp.1-18.

[7] G.C. Lazaroiu, M. Roscia, "Definition methodology for the smart cities model," *Energy*, vol. 47, No. 1, pp. 326-332, Nov. 2012.

[8] *IEEE Std. 1159:2009, IEEE Recommended Practice for Monitoring Electric Power Quality*, Jun. 2009.

[9] M. Longo, D. Zaninelli, M. Roscia and M. Costoiu, "Smart City to improve power quality," Proc. *IEEE 16th International Conference on Harmonics and Quality of Power (ICHQP), 2014*, Bucharest, Romania, May 2014, pp. 458-462.

[10] V. Monteiro, H. Gonçalves and J. L. Afonso, "Impact of Electric Vehicles on power quality in a Smart Grid context," Proc. *2011 11th International Conference on Electrical Power Quality and Utilisation (EPQU)*, Lisbon, Portugal, Oct. 2011, pp. 1-6.

[11] B. A. Ahmad, H. H. ElSheikh and A. Fadoun, "Review of power quality monitoring systems," Proc. *International Conference on Industrial Engineering and Operations Management (IEOM)*, Dubai, UAE, Mar. 2015, pp. 1-8.

[12] C. Muscas, L. Peretto, S. Sulis and R. Tinarelli, "Investigation on Multipoint Measurement Techniques for PQ Monitoring," in *IEEE Transactions on Instrumentation and Measurement*, vol. 55, no. 5, pp. 1684-1690, Oct. 2006.

[13] D. Gallo, C. Landi, M. Luiso and E. Fiorucci, "Survey on Voltage Dip Measurements in Standard Framework," in *IEEE Transactions on Instrumentation and Measurement*, vol. 63, no. 2, pp. 374-387, Feb. 2014.

[14] J. V. Milanović et al., "International Industry Practice on Power-Quality Monitoring," *IEEE Transactions on Power Delivery*, vol. 29, no. 2, pp. 934-941, Apr. 2014.

[15] A. Moschitta, P. Carbone, C. Muscas, "Generalized Likelihood Ratio Test for Voltage Dip Detection," in *IEEE Transactions on Instrumentation and Measurement*, vol. 60, no. 5, pp. 1644-1653, May 2011.

[16] M. Didden, E. De Jaeger, W. D'Haeseleer, and R. Belmans, "How to connect a voltage sag-measuring device: Phase to phase or phase to neutral?," *IEEE Transactions on Power Delivery*, vol. 20, no. 2, pp. 1174–1181, Apr., 2005.

[17] *IEC 61000-4-7:2012, Electromagnetic compatibility (EMC) - Part 4-7:General Guide on Harmonics and Interharmonics Measurements for Power Supply Systems and Equipment Connected Thereto*.

[18] *IEC 61000-4-15:2010, Electromagnetic compatibility (EMC) - Part 4-15: Testing and measurement techniques - Flickermeter - Functional and design specifications.*

[19] *IEC 61000-4-30:2015, Electromagnetic compatibility (EMC) - Part 4-30: Testing and measurement techniques – Power quality measurement methods.*

[20] A. M. Dumitrescu, R. Roman and M. Albu, "Synchronized measurements and power quality assesment," Proc. *IEEE PowerTech,* Eindhoven, Netherlands, Jun.-Jul. 2015, pp. 1-6.

[21] S. Kumar, M. K. Soni and D. K. Jain, "Power Quality Monitoring using PMU," *International Journal of Computer Applications*, vol. 135, no. 7, pp. 1-5, Feb. 2016.

[22] A. G. Phadke, "Synchronized phasor measurements-a historical overview," Proc. *IEEE/PES Transmission and Distribution Conference and Exhibition 2002: Asia Pacific*, Oct. 2002, pp. 476-479.

[23] A. von Meier, D. Culler, A. McEachern and R. Arghandeh, "Micro-synchrophasors for distribution systems," *Innovative Smart Grid Technologies Conference (ISGT), 2014 IEEE PES*, Washington, DC, 2014, pp. 1-5.

[24] S. Pappu et al., "Power Quality Analysis of a Sensitive Load Using a Phasor Measurement Unit," *IEEE Green Technologies Conference,* Tulsa, OK, USA, 2012, pp. 1-6.

[25] D. Belega and D. Petri, "Accuracy Analysis of the Multicycle Synchrophasor Estimator Provided by the Interpolated DFT Algorithm," *IEEE Trans. on Instrumentation and Measurement,* vol. 62, no. 5, pp. 942,953, May 2013.

[26] J. A. de la O Serna, "Dynamic Phasor Estimates for Power System Oscillations," *IEEE Transactions on Instrumentation and Measurement*, vol. 56, no. 5, pp. 1648-1657, Oct. 2007.

[27] M. Platas-Garza and J. A. de la O Serna, "Dynamic Phasor and Frequency Estimates Through Maximally Flat Differentiators, *IEEE Transactions on Instrumentation and Measurement*, vol. 59, no. 7, pp. 1803-1811, Jul. 2010.

[28] D. Belega, D. Macii and D. Petri, "Fast Synchrophasor Estimation by Means of Frequency-Domain and Time-Domain Algorithms," in *IEEE Transactions on Instrumentation and Measurement*, vol. 63, no. 2, pp. 388-401, Feb. 2014.

[29] EN 50160:2010, *Voltage characteristics of electricity supplied by public distribution systems*, Brussels, Belgium, Dec. 2010.

[30] G. Barchi, D. Macii, D. Belega and D. Petri, "Performance of Synchrophasor Estimators in Transient Conditions: A Comparative Analysis," *IEEE Transactions on Instrumentation and Measurement*, vol. 62, no. 9, pp. 2410-2418, Sep. 2013.